

1 **Assessment of inter-model variability and biases of the global water**  
2 **cycle in CMIP3 climate models**

3 **Beate G Liepert<sup>1</sup> and Michael Previdi<sup>2</sup>**

4 <sup>1</sup>NorthWest Research Associates, 4118 148th Ave NE, Redmond, WA 98052, USA

5 Email: [Liepert@nwra.com](mailto:Liepert@nwra.com)

6 <sup>2</sup>Lamont-Doherty Earth Observatory of Columbia University, 61 Route 9W, Palisades NY  
7 10964, USA

8 Submitted to Environmental Research Letters 8 May 2011, revised 23 September 2011

9

## Global water cycle assessment in CMIP3 climate models

9  
10  
11  
12  
13  
14  
15  
16  
17  
18  
19  
20  
21  
22  
23  
24  
25  
26  
27  
28  
29  
30  
31  
32  
33  
34  
35

### ABSTRACT

Observed changes such as increasing global temperatures and the intensification of the global water cycle in the 20<sup>th</sup> century are also robust results of coupled general circulation models (CGCMs). In spite of this success model-to-model variability and biases that are small in first order climate responses however, have implications for climate predictability especially when multi-model means are used. We show that most climate simulations of 20<sup>th</sup> and 21<sup>st</sup> century A2 scenario performed with CMIP3 (Coupled Model Intercomparison Project Phase 3) models have deficiencies in simulating the global atmospheric moisture balance. Large biases of only a few models (some biases reach the simulated global precipitation changes in the 20<sup>th</sup> and 21<sup>st</sup> century) affect the multi-model mean global moisture budget and an imbalanced flux of -0.14 Sv exists whereas the multi-model median imbalance is only -0.02 Sv. For most models, the detected imbalances furthermore change over time. As a consequence, in 13 of the 18 CMIP3 models examined, global annual mean precipitation exceeds global evaporation, indicating that there should be a “leaking” (decrease) of moisture from the atmosphere whereas for the remaining 5 models a “flooding” is implied. Nonetheless, in all models, the actual atmospheric moisture content and its variability correctly increases during the course of the 20<sup>th</sup> and 21<sup>st</sup> centuries. These discrepancies therefore imply an unphysical and hence “ghost” sink / source of atmospheric moisture in the models whose atmospheres flood / leak. The source / sink of moisture can also be regarded as atmospheric latent heating / cooling and hence as positive / negative perturbations of the atmospheric energy budget or non-radiative forcings in the range of -1 to +6 W/m<sup>2</sup> (median is +0.1 W/m<sup>2</sup>). The inter-model variability of the global atmospheric moisture transport from oceans to land areas, which impacts the terrestrial water cycle, is also quite high and ranges from 0.26 to 1.78 Sv. In the 21<sup>st</sup> century this transport to land increases by about 5% per century with a model-to-model range from 1 to 13% per century. We suggest that this variability is partially due to the different implementations of aerosol forcings in the models. The pole wards shifts of dry zones in climate simulations of the 21<sup>st</sup> century are also assessed in this study. It is shown that the multi-model means of the two subsets of models with negative and positive imbalances in the atmospheric moisture budget produce spatial shifts in the dry zone positions similar in size of the spatial shifts expected from 21<sup>st</sup> century global warming simulations. Thus, in this example of the dry zone extension, spatial multi-model means also depend on the selection of models which should be considered with caution in future analysis.

### 36 **1. Introduction**

37 As understanding of the climate system increased substantially over the years, modeling of the Earth's climate  
38 also progressed rapidly. Observed changes such as increasing global temperatures and the intensification of the  
39 water cycle are common, robust features of coupled general circulation models (CGCMs) as well as described in  
40 the 4<sup>th</sup> Assessment Report of the Intergovernmental Panel on Climate Change (IPCC-AR4). Due to these  
41 consistencies between models and observations, climate models are now widely used to predict climatic change  
42 under future anthropogenic emission scenarios. In addition to the robust results of global temperature and  
43 precipitation, CGCMs are more and more used to predict other complex climate responses of natural and  
44 anthropogenic perturbations. Such responses are for example shifts in the edge of the dry zones. Model-to-model  
45 variability that appears small in first order effects may however, have unexpected implications for more complex  
46 responses. An approach to overcome model uncertainties is suggested by Reichler and Kim (2008). They  
47 showed that for combinations of atmospheric variables, multi-model means of climate simulations represent the  
48 best estimates of the climate state when compared to 20<sup>th</sup> century observations. Their analysis was performed  
49 with data from the Coupled Model Intercomparison Project Phase 3 (CMIP3) archive. Calculating multi-model  
50 means of simulations and multi-model means of subsets of simulations became a common approach in recent  
51 years. Climate forcings, for example ozone recovery, and their climate responses were studied with multi-model  
52 means of hierarchies of models (e.g., Son et al., 2008). In this approach however, a few outlier models can skew  
53 outcomes significantly and can result in misleading conclusions. Another issue in predicting climate and source  
54 of uncertainty is that models are evaluated with 20<sup>th</sup> century observations and then used for predicting future  
55 climates. Tests that are designed independently of observations and observational uncertainty would hence be  
56 preferable.

57 Arguable the largest uncertainties in both climate observations and models stem from the hydrological cycle.  
58 While the basic processes are well known and the acceleration of the water cycle with global warming is well  
59 studied, the inter-model variability of the precipitation response and other hydrological processes remain high  
60 (Liepert and Previdi, 2009). Here we investigate these inter-model variability and biases of the global water  
61 cycle in CMIP3 models. We focus on the atmospheric branch of the hydrological cycle because it is intrinsically  
62 connected to the energy budget of the atmosphere and thus to climate forcings and feedbacks (see e.g. Liepert

## Global water cycle assessment in CMIP3 climate models

2010). The atmospheric moisture content is by far the smallest storage term in the global water cycle. Although small variations in atmospheric moisture content can play key roles in the energy balance of the planet. Latent heating redistributes energy in the vertical column and cloud formation affects the emission of infrared and reflection of solar radiation while water vapor absorbs near-infrared and infrared radiation (e.g., Hansen *et al.* 1997, and Previdi and Liepert 2011). The atmospheric moisture transport from oceans to land constitutes the moisture input to the continental freshwater cycle. Hence the atmospheric, “oceans to land” moisture transport needs to be accurately predicted for reliable climate impact assessments. Another example of the importance of the atmospheric moisture balance is that the spatial distribution of the net amount of the fluxes of precipitation and evaporation identify the boundaries of the dry zones on Earth. These processes are investigated in this study. The manuscript first describes CMIP3 model data and data handling and in the second section introduces an analysis of biases of the global atmospheric moisture balance in climate models and its implications. In the second half of the study inter-model variability of atmospheric moisture transport from oceans to land and variability of extensions of dry zones are discussed.

76

### 77 **2. Climate Modeling Data**

The climate modeling experiments analyzed here are the archived CMIP3 simulations of fully coupled ocean-atmosphere general circulation models. Investigated in this study are the 20<sup>th</sup> century scenarios with climate forcings determined by the individual modeling groups and the 21<sup>st</sup> century scenario A2. Data from all runs of 18 models were downloaded from the archive ([http://www-pcmdi.llnl.gov/ipcc/ipcc\\_data\\_status.php](http://www-pcmdi.llnl.gov/ipcc/ipcc_data_status.php)). The 21<sup>st</sup> century runs were available for only 16 of the 18 models. The data sets of the 20<sup>th</sup> and the 21<sup>st</sup> century were combined into one data set. The models are listed in Table 1 and the abbreviations that follow the IPCC-AR4 nomenclature are also listed in the footnote of Table 1. For the atmospheric moisture balance analysis we examined ensemble means of all runs for each model and one arbitrary chosen run for each model. There were no differences in outcomes of the ensemble means versus the individual runs. Hence all results presented here are based on the analysis of individual model runs. For one model the analysis was performed with daily and as monthly data. The finer temporal resolution does not change the outcome of the assessment. Hence we use monthly datasets for this study. All datasets for each model are processed in the spatial resolution provided by

## Global water cycle assessment in CMIP3 climate models

90 the modeling groups and archived in CMIP3. No re-gridding was necessary for this analysis except for the  
91 calculation of the multi-model mean dry zone distributions. Available column integrated data were obtained  
92 from the archive and no vertical integration was performed, except water vapor for one model that did not  
93 provide column integrated water vapor for the archive (see Table 1). Individual land masks for each model were  
94 used for the calculation of the ocean to land atmospheric moisture transport. In case of models with mixed land-  
95 ocean grid cells, cells with land areas larger than 50% were considered land cells. The spatial integration was  
96 performed by summation of grid cell values, which were primary multiplied with the calculated grid cell areas.  
97 The variables we obtained are the monthly means of the surface latent heat flux and the monthly mean  
98 precipitation rates for each model. Precipitation consists of solid and liquid fluxes including negative values for  
99 dew and frost. Ocean evaporation was calculated from the available surface latent heat fluxes divided by the  
100 latent heat of vaporization ( $L_{\text{vap}} = 2501 \text{ J/g}$ ) and sublimation of sea ice was calculated from the surface latent  
101 heat fluxes over sea ice divided by the latent heat of sublimation ( $L_{\text{sub}} = 2835 \text{ J/g}$ ). Evapo-transpiration and  
102 sublimation over land was calculated from the surface latent heat fluxes divided by the latent heat of  
103 vaporization ( $L_{\text{vap}} = 2501 \text{ J/g}$ ). This procedure slightly overestimates sublimation rates over land ice and snow  
104 because latent heat of vaporization is somewhat smaller than latent heat of sublimation. For one model we  
105 calculated land sublimation explicitly over ice and snow with the latent heat of sublimation and did not find  
106 accountable discrepancies after global integration. In the following we will use the expression “evaporation” for  
107 the sum of evapo-transpiration, evaporation and sublimation. From the CMIP3 archive we further obtained the  
108 archived monthly means of column-integrated water vapor for each model. For most models column integrated  
109 cloud liquid and ice water content was also available (marked in Table 1) and was added to the moisture content.  
110 The solid and liquid contributions to total atmospheric moisture are small compared to the contribution in the gas  
111 phase. Atmospheric moisture content was calculated as the sum of solid, liquid water, and water vapor.

112

### 113 3. Global Atmospheric Moisture Balance

#### 114 3.1. Method

115 According to Peixoto and Oort (1992) the moisture balance of an atmospheric column can be described in its  
116 vertically integrated form as follows:

## Global water cycle assessment in CMIP3 climate models

$$\frac{\partial W}{\partial t} + \nabla_h \bar{Q} = E - P$$

$$\text{with } \bar{Q} = \int_{z=0}^{\infty} \bar{v} \cdot q dz \quad \text{and} \quad W = \int_{z=0}^{\infty} q dz \quad (1)$$

117

118 The vector  $\bar{v}$  is the horizontal wind velocity and  $q$  the atmospheric moisture content (vapor, liquid, solid) of the

119 vertical layer  $dz$ . Integrated over the globe the horizontal moisture divergence  $\nabla_h \bar{Q}$  in the atmospheric column

120 disappears and the column integrated atmospheric moisture storage change  $\frac{\partial W}{\partial t}$  is balanced by the sources and

121 sinks of atmospheric moisture, which are the surface fluxes of evaporation minus precipitation  $E - P$ .

122 Furthermore, when applied to discrete data indexed  $i$ , the global atmospheric moisture gain or loss within the

123 time period of  $n$  time steps can be described by the net accumulation of sources  $E_i$  and sinks  $P_i$  as indicated on

124 the right side of (2):

$$\frac{\partial W}{\partial t} = E - P \Rightarrow \langle W_n - W_1 \rangle = \sum_{i=1}^n \langle E_i - P_i \rangle \quad (2)$$

125

126 This means the global mean of the atmospheric moisture content changes with the net fluxes in and out of the

127 atmosphere. For monthly modeling data this means the annual atmospheric moisture gain/loss (e.g., from

128 January to December or any other 12-month period) is balanced by the yearlong net accumulation of monthly  $E_i$

129 minus  $P_i$ .

$$\text{Res} = E - P - \frac{\partial W}{\partial t} \Rightarrow \text{Res}(y) \equiv \sum_{i=1}^{12} \langle E_i - P_i \rangle - \langle W_{12} - W_1 \rangle \quad (3)$$

130

131 Thus for the annual atmospheric moisture budget, a potential residual or imbalance  $Res$  for the year  $y$  can be

132 calculated and a time series of these annual residuals can be constructed.

133

### 134 3.2. Results

135 Figure 1 summarizes the 20<sup>th</sup> to 21<sup>st</sup> century long-term annual means and inter-annual variability of the two

136 components of the atmospheric moisture balance for each CMIP3 model. The inter-annual variability in all cases

137 is calculated as standard deviation of the annual means after the trends of the data records were removed. The

138 units for all moisture fluxes considered here are in Sverdrup (1 Sverdrup = 1 Sv =  $10^6 \text{ m}^3 \text{ s}^{-1} = 31.6 * 10^{12} \text{ m}^3 \text{ a}^{-1}$ ).

## Global water cycle assessment in CMIP3 climate models

139 Illustrated in Figure 1 in red error bars is the inter-annual variability of the time series of  $\frac{\partial W}{dt}$ . Not recognizable  
140 in Figure 1 are the mean annual atmospheric moisture changes. The long-term multi-model mean of moisture  
141 change within the year is 0.00048 Sv. A positive, albeit small, increase like this is expected due to the increasing  
142 moisture-holding capacity of the atmosphere with global warming. An increase in global atmospheric moisture  
143 content  $W$  of about  $3.03 * 10^{12} \text{ m}^3$  over the 200-year period can be calculated from the multi-model mean of these  
144 data. These changes in atmospheric moisture content are small compared to other storage terms of the water  
145 cycle. Nonetheless the atmospheric moisture increases are important in the climate system because they initiate  
146 the radiative water vapor and cloud feedback.

147 Also shown in Figure 1 are the long-term annual means of the time series of  $E - P$  in columns and their inter-  
148 annual variability in error bars, both in blue. Mean  $E - P$  values exceed the actual variability of moisture storage  
149 changes  $\frac{\partial W}{dt}$  (red error bars) in almost all models and hence result in unbalanced moisture budgets (3). The  
150 analysis was repeated with all available simulations and no differences in the results were obtained. As  
151 mentioned before, the original data are only multiplied with grid cell areas before summation. Hence it is  
152 unlikely that numerical errors from the integration can cause these residuals. Also mentioned in the data section  
153 are missing cloud ice water content data for some models as well as the treatment of land sublimation as  
154 evaporation. We further tested the possible biases due to these uncertainties with one model that includes all data  
155 records. Omitting these data could not account for the observed deficiencies.

156 The long-term means, inter-annual variability and long-term trends of the residuals are also listed in Table 1. It is  
157 clear that some models have balanced atmospheric moisture budgets. For example the model CGCM3.1 (T47),  
158 which is flux corrected (marked with "\*" in Table 1), closes the atmospheric moisture budget, while other  
159 models (CSIRO-MK3.0 and UKMO-HadCM3) that are without flux adjustments are also in closure within the  
160 uncertainty range (information on flux adjustments was taken from IPCC-AR4 2007 Table 8.1). Positive biases  
161 could be identified for five and negative biases for thirteen models. Negative  $E - P$  values in Table 1 and Figure  
162 1 indicate a "leaking" ("drying") of moisture from the atmosphere and positive  $E - P$  indicates a "flooding"  
163 ("moistening") of the model atmospheres. The multi-model mean is negative with -0.14 Sv. The residuals are

## Global water cycle assessment in CMIP3 climate models

164 generally small compared to the calculated global annual mean precipitation trends of the 20<sup>th</sup> and 21<sup>st</sup> century.  
165 The results of each model are listed in Table 1. Although, the unphysical multi-model mean drying is about one  
166 third the size of the multi-model mean precipitation trend (Table 1). This is the case because for a few models  
167 the biases are large and can reach the magnitude of the inter-annual variability of precipitation. Consequently the  
168 multi-model median of the residuals of -0.02 Sv is more appropriate. It is important to point out that the leaking  
169 or flooding of the atmosphere that is anticipated based on the global imbalances of  $E$  and  $P$  is not reflected in the  
170 actual simulated atmospheric moisture content  $W$  and its inter-annual variation  $\frac{\partial W}{\partial t}$  as discussed above and  
171 shown in Figure 1. In the flooding models, the actually simulated moisture content changes  $\frac{\partial W}{\partial t}$  are  
172 significantly smaller than would be expected from the modeled  $E - P$ , whereas in the leaking models the  
173 simulated increases of  $\frac{\partial W}{\partial t}$  are of opposite sign than expected from the modeled  $E - P$ . This therefore implies  
174 an artificial or unphysical source of atmospheric moisture in the models that leak and an unphysical sink in the  
175 models that flood appear.  
176 In general the global atmospheric moisture imbalances are small compared to precipitation and other fluxes in  
177 the global water cycle. They are also not unexpected in climate models (see e.g., Rodriguez *et al.* 2010 and  
178 Kavetski and Clark 2010). These small biases in atmospheric moisture however, become important if we  
179 consider them as perturbation of the atmospheric energy budget. Additional moisture translates into excessive  
180 latent heat release into the atmosphere through phase transition in precipitation formation (see also Edwards  
181 2007). The atmosphere responds to this “ghost” latent heating with various feedback processes, which cannot be  
182 identified easily. Hence the artificial source of moisture can be interpreted as “instantaneous”, non-radiative  
183 forcing of the energy balance. Table 1 lists the “excess latent heat” for each model, which are in the range of -1  
184 to +6 W/m<sup>2</sup> with a small positive multi-model median of +0.1 W/m<sup>2</sup>.  
185 Climate predictions of water cycle strength however, are not necessarily influenced by biases, because  
186 considered in climate model analyses are often differences of two climate states or changes over time from a  
187 control run. Changes over time (drifts) of these biases however, would influence climate predictions of water  
188 cycle strength. Tendencies of biases in each model calculated as linear trends for the annual residuals are listed



189 in Table 1. This analysis reveals drifts of the moisture imbalances. Tendencies, positive or negative, occur in the  
 190 residuals of most models as illustrated in Figure 2 where the initial imbalance of each run is removed. The drifts  
 191 are generally negligible compared to e.g., global precipitation trends (see Table 1). For some models however,  
 192 the trend in the residuals can be as large as five percent of predicted precipitation changes. For one climate  
 193 model the bias drift is double the precipitation trend of the 100-year period. Consequently multi-model means of  
 194 global precipitation trends should be considered with caution and multi-model medians are more reliable.

195

#### 196 4. Global Atmospheric Moisture Transport from Oceans to Land

##### 197 4.1. Method

198 As mentioned in the introduction the connection between land and ocean water cycles is important for many  
 199 applications. The net atmospheric moisture transport from oceans to land connects ocean fresh water cycle and  
 200 land hydrology. The water cycle is eventually closed by continental runoff, which is the return flow. Here we  
 201 investigate the inter-model variability of the net atmospheric moisture transport from oceans to land to assess the  
 202 uncertainty of this parameter of significant climatic change impact. Atmospheric moisture transport is commonly  
 203 calculated as atmospheric moisture convergence with 3-dimensional wind and moisture fields (1). Because of the  
 204 potentially high numerical uncertainty in calculating vertically integrated convergence directly we chose the  
 205 more indirect atmospheric moisture budget approach. The atmospheric moisture supply for all land areas is  
 206 derived from the moisture budget over the oceans.

$$207 \quad \oiint_{\partial \mathcal{O}_c} d\vec{S} \cdot \vec{Q} = \iiint_{\mathcal{O}_c} \nabla \cdot \vec{Q} dV = \iiint_{\mathcal{O}_c} \left( +E - P - \frac{\partial W}{\partial t} \right) dV \quad (4)$$

208 The left side of (4) describes the integration of the Gauss's flux theorem. Horizontal moisture flux  $\vec{Q}$  through the  
 209 surfaces  $d\vec{S}$  of the entire atmospheric columns over the oceans is equal to the moisture convergence in the  
 210 volumes  $dV$  of the atmospheric columns over the oceans. This is the case because fluxes through the air-sea  
 211 boundary are  $E$  and  $P$  while the fluxes at the top of the atmosphere are expected to be zero. The moisture  
 212 convergence can then be replaced by the atmospheric moisture budget of (1). The globally integrated  
 213 formulation of the atmospheric moisture transport from oceans to land is therefore:

## Global water cycle assessment in CMIP3 climate models

$$214 \quad \iint_{\partial O_c} d\vec{S} \cdot \vec{Q} = \left\langle \frac{\partial W}{\partial t} + E - P \right\rangle_{O_c} \quad (5)$$

215 The brackets  $\langle \rangle_{O_c}$  symbolize the integration of all columns over the ocean areas. With (5), annual atmospheric  
216 moisture transports from oceans to land can then be calculated for all CMIP3 climate models.

217

### 218 **4.2. Results**

219 As pointed out in Table 1 the long-term, average atmospheric moisture transport from oceans to land varies quite  
220 significantly from model to model with a range from 0.26Sv to 1.78Sv. The multi-model mean of 1.1 Sv and  
221 median of 1.2 Sv for the 20<sup>th</sup> and 21<sup>st</sup> century simulations however, remain close to the observational estimate of  
222 1.2Sv (e.g., Baumgartner and Reichel 1979). The inter-annual variability (calculated as standard deviation after  
223 the record was detrended) is on average about 5-6% of the total transport in the models. In CMIP3 models, most  
224 of the long-term variability stems from underlying trends towards increasing moisture transport to land areas.

225 The linear trends in moisture transports from oceans to land areas in the 20<sup>th</sup> and 21<sup>st</sup> century are shown in Figure  
226 3. Overall, land areas will receive on average about 0.04-0.05 Sv (about 4%) more moisture per 100 years from  
227 the oceans through atmospheric transport. This increase amounts to an extra moisture input to land of about the  
228 size of the discharge of the River Nile per hundred years (e.g., Gupta 2007). In the models CCSM3 and ECHO-  
229 G, the intensified moisture transports reach up to 0.13 Sv in 100 years or an increase of 10% of the total  
230 atmospheric, ocean to land transport.

231 Further shown in Figure 3 are the linear trends of the residuals of the atmospheric moisture balances of  
232 simulations of the 20<sup>th</sup> and 21<sup>st</sup> centuries (Table 1). In Figure 3 the two models (CNRM-CM3 and FGOALS-  
233 g1.0) with reduced atmospheric moisture transport are also the models with strong increasing artificial leaking  
234 from model atmospheres. The median of the drifts in atmospheric moisture balances is coincidentally zero due to  
235 compensation amongst models. Arguably drifts in the atmospheric moisture imbalance could affect the  
236 atmospheric moisture transport from oceans to land areas because the largest flux in the global water cycle is  
237 ocean evaporation. In general however, the trends in the global residuals are small compared to the trends in  
238 atmospheric moisture transport (see multi-model mean and median in Figure 3).

239

## 240 5. Extension of the Dry Zone Edges

### 241 5.1. Method

242 Several approaches exist for identifying the edges of the dry zones in the subtropics (see Seidel *et al.* 2008 for an  
243 overview). For example, the descending branch of the Hadley circulation determines the edges of the subsidence  
244 region, which can be identified as the position of the jet streams or the zero net flow of mass from north to south  
245 in the lower atmosphere. Other distinct characteristics such as the stratospheric Brewer-Dobson circulation  
246 realized in the stratospheric ozone distribution or the tropopause height identify the width of the tropics and  
247 hence the edges of the dry zones as well. The ascending branch of the Hadley cell also produces cloud bands  
248 whose edges mark the beginning of the dry zone. The gradient of outgoing long-wave radiation is used for this  
249 approach. At the surface, dry zones are regions with evaporation exceeding precipitation and the edges are the  
250 zero contour line of  $E - P$  or  $E = P$ . This definition has been used in observations and modeling studies (see e.g.,  
251 Previdi and Liepert 2007).

252

### 253 5.2. Results

254 Figure 4a shows the  $E = P$  contours for all CMIP3 models in light blue or light red color. Models with negative  
255 residuals in the moisture budget are marked in red and with positive residuals in blue. The inter-model variability  
256 of the dry zones is large. We further separate the models into two subsets. Dry zone edges in bold colors  
257 represent the multi-model composites of the two model subsets. The group with artificially leaking atmospheres  
258 is in bold red whereas the artificially flooding modeling group is marked in bold blue. As illustrated in Figure 4a  
259 the inter-model variability of the subsets is still significant. The “leaking model-composite” seems to reveal  
260 slightly narrower dry zone areas in the Northern and Southern Pacific particularly on the pole-ward edge  
261 compared to the flooding model-composite. The dry zones of the “leaking-models” are also slightly smaller in  
262 extent over the continents. Differences in the Eastern Pacific Walker circulation are recognizable with a zonal  
263 stretched descending branch in the tropical Pacific in the flooding models. The pattern indicates a more  
264 pronounced double ITCZ when the models’ atmospheres experience positive biases.

265 In a former study (Previdi and Liepert 2007) we found as a robust result of all CMIP3 models the pole-ward  
266 extensions of the dry zone edges of about 1 degree of latitude on average with 21<sup>st</sup> century global warming. The

## Global water cycle assessment in CMIP3 climate models

267 formerly published pole-ward extensions are reproduced for the CMIP3 models in Figure 4b as well. The mean  
268 spatial distributions of the dry zones of the first 20-year period and the last 20-year period of the 21<sup>st</sup> century are  
269 shown in Figure 4b in blue and green respectively with the multi-model mean contours in bold. The inter-model  
270 variability of the dry zone edges for the predictions is again quite large and the shifts in dry zone edges in the  
271 21<sup>st</sup> century are similarly to the differences of the two subsets of the climate models with different biases. The  
272 differences and shifts can be clearer shown as zonal averages, because of the latitudinal structures of the  $E - P$   
273 fields. Zonal averaging was performed as follows: grid cell values with precipitation > evaporation (“wet” cells)  
274 were set to the discrete value ‘zero’ and grid cell values with evaporation  $\geq$  precipitation (“dry” cells) were set to  
275 ‘one’. These fields of discrete values were then zonal averaged. A zonal average of zero means the latitude band  
276 is outside the dry zone.

277 Figure 5 shows the results of this analysis for the combination of the negative and positive residual subsets and  
278 the two 20-year time intervals of the 21<sup>st</sup> century predictions of the models. The first and the last 20-year period  
279 of the leaking models are in solid and dashed lines, shown in red, and the first and last 20-year period of the  
280 flooding models are shown in solid (2001-2020) and dashed (2081-2100) lines shown in blue. The spreads  
281 between the models (not shown) are quite large for both, the biases and the prediction trends, particularly in the  
282 tropical belt. For the composites of the two modeling groups a narrower tropical rain belt (from around 15°S to  
283 15°N) for the (red) leaking average s recognizable at the equator side of the southern hemisphere. The  
284 differences at the pole-ward edges of the subtropical dry zones are not as pronounced. Interestingly, for the  
285 (blue) flooding model composite the mid-latitude storm-track and polar region (50° – 80°N and 60° – 80°S) are  
286 more populated and hence drier compared to the leaking model atmospheres. In these zonal bands the model  
287 differences are larger then the 21<sup>st</sup> century shifts.

288 The pole-ward shift of the dry zone maximum extent is more prominent in the southern hemisphere. It is  
289 noteworthy that the overall magnitude of differences is similar in both comparisons but the climate change signal  
290 of shifting dry and wet zones, remains qualitatively the same for both bias groups. The strengths of the shifts are  
291 different between the subgroups.

292 We also calculated the areal extent of the dry zones as fraction of the total area of the globe, which indicates  
293 whether the dry zones are shrinking, expanding or just shifting. In Table 2 the areal fractions of the dry zones

## Global water cycle assessment in CMIP3 climate models

294 show no significant differences between the two bias composites. The dry zones cover on average about 40% of  
295 the globe in these models. The calculation is repeated with the A2 scenario global warming experiments. The  
296 differences in areal sizes of the dry zones between the first two and the last two decades of the 21<sup>st</sup> century also  
297 reveal no significant tendencies. In ten models the dry zones shrink slightly and in six models an equally small  
298 extension (less than one percent) is indicated. The models with negative or positive net moisture budgets do not  
299 show any preference for shrinking or expanding hence the areal fraction of the dry zones seems a robust feature  
300 of the climate system similar to the global mean relative humidity.

301

### 302 **6. Discussion and Conclusions**

303 In this study we assessed global atmospheric moisture budgets in CMIP3 climate model simulations of the 20<sup>th</sup>  
304 and 21<sup>st</sup> century scenario A2. For these models Reichler and Kim (2008) showed that for combinations of  
305 atmospheric variables the multi-model means represent the best estimates of the climate state when compared to  
306 20<sup>th</sup> century observations. Based on our investigations, we suggest that for water cycle variables like  
307 precipitation or  $E - P$  however, a few models can bias multi-model means. The inter-model variability is reduced  
308 when the multi-model median is used. We conclude this from the global atmospheric moisture budget, which is  
309 out of balance by -0.14 Sverdrup in the multi-model mean whereas the multi-model median is only out of  
310 balance by -0.02 Sv. The discrepancies in the moisture balance vary hugely amongst models and range from -  
311 1.34 to 0.20 Sv. The biases are also not constant over time and can drift significantly. Positive and negative drifts  
312 were detected for the simulations of the 20<sup>th</sup> and 21<sup>st</sup> century. The trends in the model biases range from a few  
313 percent of simulated global precipitation trends to less than a tenth of a percent. For one model the trend in the  
314 bias is 200% of the predicted precipitation change in a 100-year period. Hence models with large drifts should be  
315 excluded from multi-model mean calculations.

316 The global biases in moisture balance can also be regarded as artificial “leaking” of moisture from the  
317 atmosphere when the imbalances are negative (which is the case in thirteen of the eighteen models). This  
318 leaking is artificial in the sense that the actual moisture content of the atmosphere is simulated to increase during  
319 the 20<sup>th</sup> and 21<sup>st</sup> centuries. Thus, discrepancies between the simulated  $\frac{\partial W}{\partial t}$  and  $E - P$  implies an unphysical,

## Global water cycle assessment in CMIP3 climate models

320 “ghost” source of moisture. This “ghost” moisture source can also be described as excess latent heating in the  
321 energy budget of the atmosphere and therefore as climate perturbation or non-radiative “ghost” forcing. The  
322 excess latent heating ranges from -1 to +6 W/m<sup>2</sup>, with a small multi-model median of +0.1 W/m<sup>2</sup>. Radiative  
323 forcings of non-CO<sub>2</sub> greenhouse gases are in the same size range.

324 The model-to-model variability of atmospheric moisture transport from oceans to land is quite high and ranges  
325 from 0.26 to 1.78 Sv, while the inter-annual standard deviations are around 0.06 Sv in the 20<sup>th</sup> and 21<sup>st</sup> century  
326 scenarios. The global flux is  $1.2 \pm 0.3$  Sverdrup (Sv) in the multi-model mean, which matches observations quite  
327 well (Baumgartner and Reichel, 1975; Schanze et al., 2010). The changes over the 100-year time period are all  
328 positive (except the two models with strongly drifting imbalances). Based on our study we expect that land areas  
329 receive on average about 4% more moisture in the next century with 0.08 Sv in the 21<sup>st</sup> century. This is about  
330 half of the observed drainage of a major river such as the Lena in Siberia that has an annual runoff of 0.17 Sv  
331 (see e.g., Gupta 2007). A reason for the inter-model variability of the moisture transport might be representation  
332 of non-GHG forcings in the models. In Liepert and Previdi (2009) we suggested that some of the discrepancies  
333 noted in precipitation changes between models and observations may be due to the various ways natural and  
334 anthropogenic aerosols are treated in IPCC-AR4 climate models. Here we use the same hypothesis for the  
335 moisture transport. Two special 20<sup>th</sup> century runs of the GISS-ER fully coupled model (prepared for IPCC-AR4)  
336 were used where anthropogenic forcings were introduced individually (see Hansen *et al.* 2005). In this model  
337 version the global atmospheric moisture budget is almost balanced and no drift over time could be detected. The  
338 atmospheric moisture transports from oceans to land is calculated from outputs of the control (i.e., unforced) run  
339 ‘CTL’, the 20<sup>th</sup> century anthropogenic greenhouse gases only ‘GHG’ and of the 20<sup>th</sup> century anthropogenic  
340 aerosols ‘AER’ (including direct and indirect effects) experiments. The aerosol forcing is spatially and  
341 temporally non-homogeneous. The GISS model results lie well within the variability of the models shown in  
342 Figure 3. The resulting atmospheric moisture transports from oceans to land in the 20<sup>th</sup> century are 0.90 Sv in the  
343 control run, 0.95 Sv in the GHG and 0.99 Sv in the Aerosol experiment. The moisture transport to land areas  
344 increases with 0.13 Sv per 100 years in the GHG and only 0.06 Sv per 100 years in the Aerosol experiment in  
345 spite of a similar sized, albeit opposite in sign, response of the surface radiative energy budget (Romanou et al.,  
346 2007). This result suggests that the treatment of aerosols in climate models affects the atmospheric moisture

## Global water cycle assessment in CMIP3 climate models

347 transport from oceans to land differently than GHG forcings and may cause some of the model-to-model  
348 variability.

349 The analysis of the dry zone extension reveals large model-to-model variability as well. The differences in  
350 spatial pattern between model groups with positive and negative moisture imbalances are comparable to the  
351 differences in the predicted pattern due to climate changes in the 21<sup>st</sup> century. Simulated pole-ward shifts of dry  
352 zones hence are dependent on the selection of models used for the analysis and these multi-model assessments  
353 should be evaluated with caution. The current study has not addressed the possible causes of the biases, which is  
354 beyond the scope of the manuscript. This question is subject of ongoing and future research and will be  
355 published at a later time.

356

### 357 *Acknowledgements:*

358 The authors thank the modeling groups for making their model output available for analysis, the Program for  
359 Climate Model Diagnosis and Intercomparison (PCMDI) for collecting and archiving this data, and the WCRP's  
360 Working Group on Coupled Modeling (WGCM) for organizing the model data analysis activity. The WCRP  
361 CMIP3 multi-model dataset is supported by the Office of Science, U.S. Department of Energy. This work was  
362 sponsored by NASA-MAP Program grant #NNG06GC66G and NSF Antarctic Oceans and Atmospheric  
363 Sciences grant #0944103. We thank Reto Ruedi, and Ken Lo for providing the NASA-GISS model simulations  
364 and the reviewers for their insightful comments.

## Global water cycle assessment in CMIP3 climate models

### 365 References

- 366 Baumgartner A, and Reichel E 1975 The world water balance: mean annual global, continental and maritime  
367 precipitation, evaporation and run-off, *Elsevier Scientific Pub. Co.*
- 368 Edwards, J M 2007 Oceanic latent heat fluxes: Consistency with the atmospheric hydrological and energy cycles  
369 and general circulation modeling, *J. Geophys. Res.* **112(D6)** D06115
- 370 Gupta, A 2007 Large rivers: geomorphology and management John Wiley, Chichester, England; Hoboken, NJ.
- 371 Hansen J, Sato M, and Ruedy R 1997 Radiative forcing and climate response *J. Geophys. Res.* **102(D6)** 6831-  
372 6864
- 373 Hansen J, and coauthors 2005 Efficacy of climate forcings *J. Geophys. Res.* **110(D18)** D18104
- 374 IPCC-AR4 2007 Contribution of working group I to the fourth assessment report of the intergovernmental panel  
375 on climate change, Solomon S, Qin D, Manning M, Chen Z, Marquis M, Averyt K B, Tignor M and Miller H L  
376 (eds.) Cambridge University Press Cambridge United Kingdom and New York NY USA
- 377 Kavetski D, and Clark M P 2010 Ancient numerical daemons of conceptual hydrological modeling: 2. Impact of  
378 time stepping schemes on model analysis and prediction, *Water Resour. Res.* **46(10)** W10511
- 379 Liepert, B G 2010 The Physical Concept of Climate Forcing, *Wiley Interdisciplinary Reviews: Climate Change.*  
380 **1** 786-802 doi:10.1002/wcc.75
- 381 Liepert B G, and Previdi M 2009 Do models and observations disagree on the rainfall response to global  
382 warming? *J. Climate* **22(11)** 3156-3166
- 383 Peixoto, J P and Oort A H 1992 Physics of climate American Institute of Physics New York
- 384 Previdi, M and Liepert B G 2007 Annular modes and Hadley cell expansion under global warming *Geophys.*  
385 *Res. Lett.* **34(22)** L22701
- 386 Previdi M, and Liepert B 2011 Climate sensitivity and the global water cycle *Climate Dynamics* submitted
- 387 Rodríguez J, Johns T, Thorpe R and Wiltshire A 2010 Using moisture conservation to evaluate oceanic surface  
388 freshwater fluxes in climate models *Climate Dynamics* 1-15
- 389 Romanou A, Liepert B, Schmidt G A, Rossow W B, Ruedy R A and Zhang Y 2007 20th century changes in  
390 surface solar irradiance in simulations and observations *Geophys. Res. Lett.* **34(5)** L05713
- 391 Schanze J J, Schmitt R W, Yu L L 2010 The global oceanic freshwater cycle: A state-of-the-art quantification  
392 *Journal of Marine Research* **68** 569-595
- 393 Seidel D J, Fu Q, Randel W J and Reichler T J 2008 Widening of the tropical belt in a changing climate *Nature*  
394 *Geosci* **1(1)** 21-24



## Global water cycle assessment in CMIP3 climate models

395 Son S W, L M Polvani, D W Waugh and CCMVal co-authors 2008 The impact of stratospheric ozone recovery  
396 on the Southern Hemisphere westerly jet *Science* **320** 1486-1489 doi: 10.1126/science.1155939  
397

## Global water cycle assessment in CMIP3 climate models

397 **Table 1.** Global annual means, inter-annual variability and trends of residuals of the atmospheric moisture  
 398 balance  $Res = \left( E - P - \frac{\partial W}{\partial t} \right)$  as described in (3) for CMIP3 climate models. Listed are global annual means and  
 399 standard deviations for the model time series of the 20<sup>th</sup> and 21<sup>st</sup> scenario A2. Also listed are global  
 400 precipitation ( $P$ ) trends and the percentage of residual ( $Res$ ) trend to precipitation ( $P$ ) trend for the same  
 401 simulations. The excess latent heating that corresponds to the moisture imbalance is given in  $Wm^{-2}$ . Models  
 402 with flux correction are marked with \*, no cloud ice data available \*\*, and models without cloud ice/water  
 403 data are marked with \*\*\*.

404

CMIP3 Model*	Mean $\pm$ Std.dev. $Res = \left( E - P - \frac{\partial W}{\partial t} \right)$ (Sv)	Trend $Res = \left( E - P - \frac{\partial W}{\partial t} \right)$ (Sv/100yr)	Trend $P$ (Sv/100yr)	Trend $Res$ / Trend $P$ %	Excess Latent Heat ( $Wm^{-2}$ )
BCCR-BCM2.0	-0.453 $\pm$ 0.010	-0.010	0.41	-2.44	-2.22
CCSM3	-0.018 $\pm$ 0.006	-0.000	0.53	-0.06	-0.09
CGCM3.1(T47)*	-0.005 $\pm$ 0.005	-0.002	0.53	-0.36	-0.03
CNRM-CM3	-0.752 $\pm$ 0.013	-0.027	0.48	-5.51	-3.69
CSIRO-MK3.0	0.007 $\pm$ 0.006	0.004	0.28	1.52	0.03
ECHAM5-MPI-OM	-0.053 $\pm$ 0.007	-0.001	0.40	-0.16	-0.26
ECHO-G**	0.053 $\pm$ 0.006	0.006	0.20	2.93	0.26
FGOALS-g1.0	-1.339 $\pm$ 0.020	-0.044	-0.02	199.19	-6.56
GFDL-CM2.0	0.014 $\pm$ 0.005	-0.005	0.16	-3.34	0.07
GISS-EH	-0.013 $\pm$ 0.004	-0.000	-0.02	0.38	-0.06
GISS-ER	-0.022 $\pm$ 0.004	0.001	0.36	0.29	-0.11
INM-CM3.0*	-0.065 $\pm$ 0.005	0.007	0.66	1.07	-0.32
IPSL-CM4	0.198 $\pm$ 0.005	-0.007	0.56	-1.25	0.97
MIROC3.2(medres)	-0.019 $\pm$ 0.006	-0.001	0.09	-1.16	-0.09
MRI-CGCM2.3.2***	-0.079 $\pm$ 0.009	0.009	0.50	1.84	-0.39
PCM (NCAR)***	-0.022 $\pm$ 0.005	0.001	0.40	0.18	-0.11
UKMO-HadCM3	0.003 $\pm$ 0.005	-0.000	0.25	-0.08	0.02
UKMO-HadGEM1	-0.017 $\pm$ 0.005	0.000	0.09	0.22	-0.09
Mean	-0.136 $\pm$ 0.009	-0.004	0.32	-	-0.70
Median	-0.018 $\pm$ 0.006	-0.000	0.38	-	-0.09

405

406

407

408

409

\*  
 BCCR-BCM2.0, 2005 Bjerknes Centre for Climate Research, Norway  
 CCSM3, 2005 National Center for Atmospheric Research, USA  
 CGCM3.1(T47), 2005 Canadian Centre for Climate Modelling and Analysis, Canada  
 CNRM-CM3, 2004 Météo-France/Centre National de Recherches Météorologiques, France

## Global water cycle assessment in CMIP3 climate models

410 CSIRO-MK3.0, 2001 Commonwealth Scientific and Industrial Research Organisation (CSIRO) Atmospheric  
411 Research, Australia  
412 ECHAM5/MPI-OM, 2005 Max Planck Institute for Meteorology, Germany  
413 ECHO-G, 2004 Meteorological Institute of the University of Bonn, Germany  
414 FGOALS-g1.0, 2004 National Key Laboratory of Numerical Modeling for Atmospheric Sciences and  
415 Geophysical Fluid Dynamics (LASG)/Institute of Atmospheric Physics, China  
416 GFDL-CM2.0, 2005 U.S. Department of Commerce/National Oceanic and Atmospheric Administration  
417 (NOAA)/Geophysical Fluid Dynamics Laboratory (GFDL), USA  
418 GISS-EH, 2004 NASA/GISS, USA  
419 GISS-ER, 2004 NASA/GISS, USA  
420 INM-CM3.0, 2004 Institute for Numerical Mathematics, Russia  
421 IPSL-CM4, 2005 Institut Pierre Simon Laplace, France  
422 MIROC3.2(medres), 2004 Center for Climate System Research (University of Tokyo), National Institute for  
423 Environmental Studies, and Frontier Research Center for Global Change (JAMSTEC), Japan  
424 MRI-CGCM2.3.2, 2003 Meteorological Research Institute, Japan  
425 PCM, 1998 National Center for Atmospheric Research, USA  
426 UKMO-HadCM3, 1997 Hadley Centre for Climate Prediction and Research/Met Office, UK  
427 UKMO-HadGEM1, 2004 Hadley Centre for Climate Prediction and Research/Met Office, UK  
428

## Global water cycle assessment in CMIP3 climate models

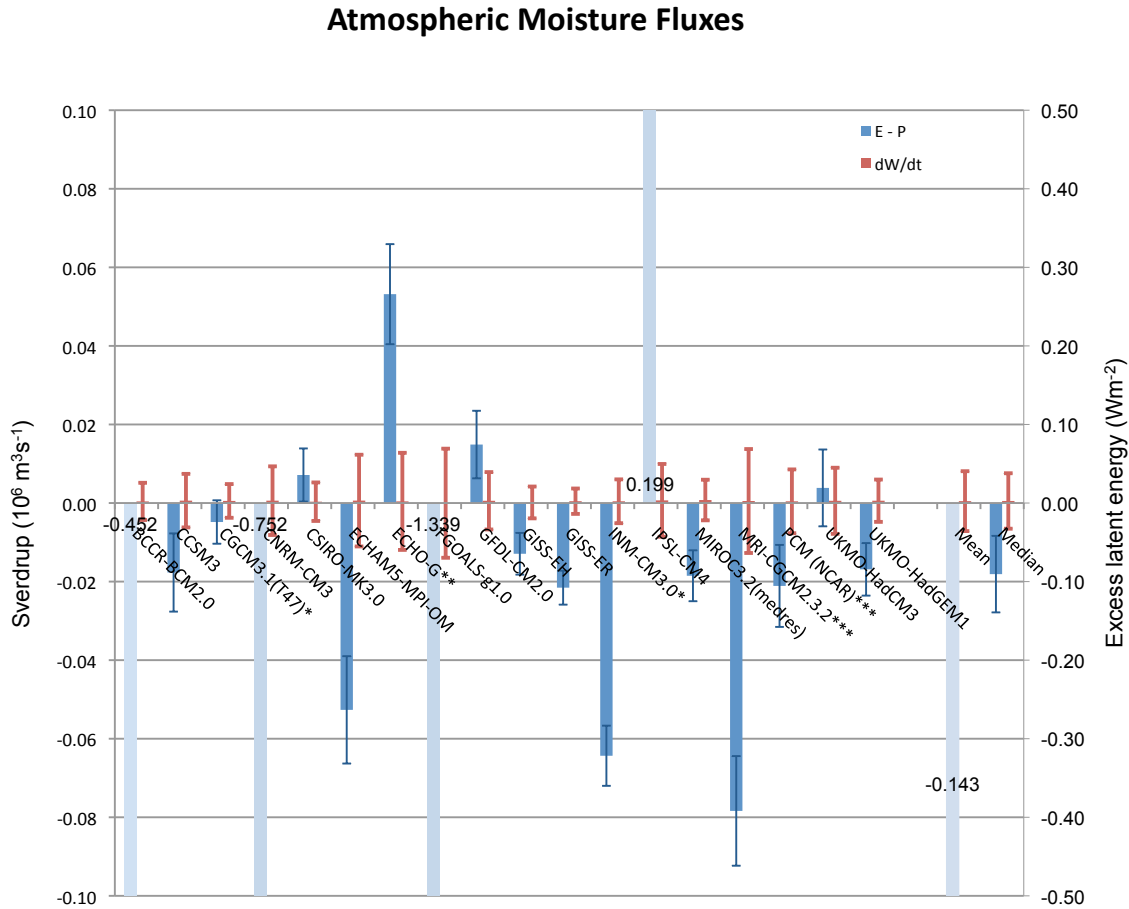
428  
 429 **Table 2.** Global annual means, inter-annual variability and trends of atmospheric moisture transport from ocean  
 430 to land areas as described in (5) for CMIP3 climate models. Listed are global annual means and standard  
 431 deviations for the model time series of the combined 20<sup>th</sup> and 21<sup>st</sup> scenario A2. Further listed is the area of the  
 432 dry zones as fractions of the area of the globe for the first 20-year period of the 21<sup>st</sup> century scenario A2. The  
 433 difference in global area fraction of the dry zones between the first (2001-2020) and the last (2081-2100) 20-year  
 434 period are also listed.

CMIP3 Model	Mean $\pm$ std.dev. Atm. moisture transport ocean-land (Sv)	Trend Atm. moisture transport ocean-land (Sv/100yr)	Mean (2001 – 2020) Global dry zone area fraction	Difference (2001-2020) – (2081-2100) Global dry zone area fraction
BCCR-BCM2.0	1.01 $\pm$ 0.04	0.04	0.406	-0.005
CCSM3	1.44 $\pm$ 0.05	0.13	0.391	-0.002
CGCM3.1(T47)*	1.32 $\pm$ 0.04	0.06	0.406	-0.002
CNRM-CM3	0.55 $\pm$ 0.05	-0.01	0.385	-0.006
CSIRO-MK3.0	1.02 $\pm$ 0.04	0.02	0.411	-0.005
ECHAM5-MPI-OM	0.96 $\pm$ 0.05	0.04	0.395	-0.030
ECHO-G**	1.21 $\pm$ 0.06	0.11	0.365	0.009
FGOALS-g1.0	0.26 $\pm$ 0.06	-0.05	No data	No data
GFDL-CM2.0	1.25 $\pm$ 0.06	0.01	0.403	-0.012
GISS-EH	1.18 $\pm$ 0.03	0.02	No data	No data
GISS-ER	1.78 $\pm$ 0.05	0.08	0.398	-0.011
INM-CM3.0*	1.11 $\pm$ 0.05	0.09	0.404	0.008
IPSL-CM4	1.44 $\pm$ 0.04	0.08	0.409	0.007
MIROC3.2(medres)	1.20 $\pm$ 0.07	0.02	0.378	0.012
MRI-CGCM2.3.2***	1.29 $\pm$ 0.12	0.01	0.401	0.004
PCM (NCAR)***	1.12 $\pm$ 0.04	0.06	0.442	0.001
UKMO-HadCM3	1.25 $\pm$ 0.06	0.08	0.391	-0.004
UKMO-HadGEM1	1.27 $\pm$ 0.06	0.02	0.417	-0.008
Mean	1.15 $\pm$ 0.07	0.05	0.400	-0.002
Median	1.21 $\pm$ 0.06	0.04	0.403	-0.006

435

436

436



437

438

**Figure 1.** Global atmospheric moisture fluxes  $E - P$  in blue and moisture content change  $\frac{\partial W}{\partial t}$  in red

439

for CMIP3 climate models. Shown are long-term annual means in columns and standard deviations in

440

error bars. The calculations were performed with the time series of the 20<sup>th</sup> and 21<sup>st</sup> scenarios A2. The

441

light blue columns are too large to be shown but the corresponding values are given on the column.

442

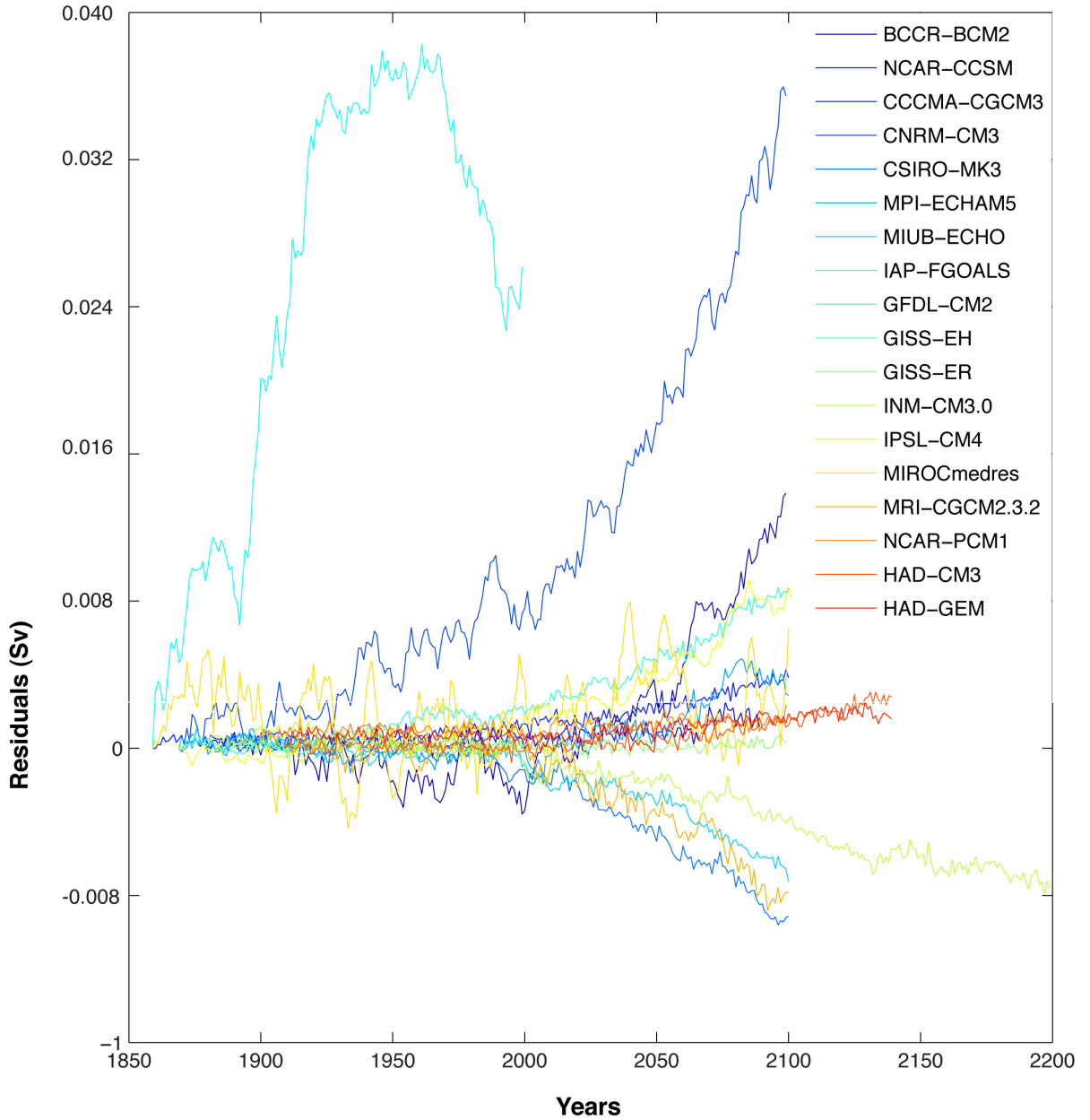
Note that models with flux correction are marked with \*, without cloud ice with \*\*, and without cloud

443

ice and water with \*\*\*.

444

444



445

446

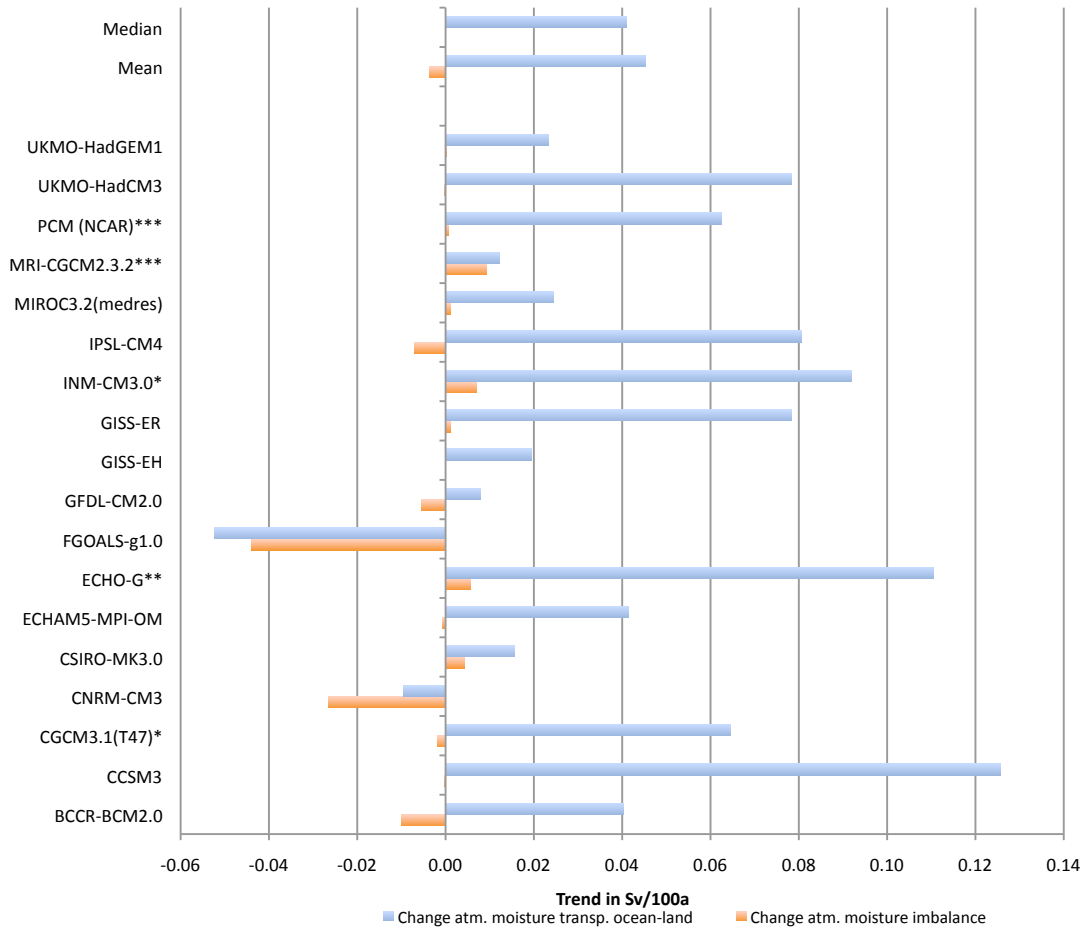
447

448

449

**Figure 2.** Global atmospheric moisture imbalances in CMIP3 climate models. Shown are time series of annual means for the 20th and 21st scenarios A2 combined. The initial imbalances were removed from the time series. The residuals are given in Sverdrup.

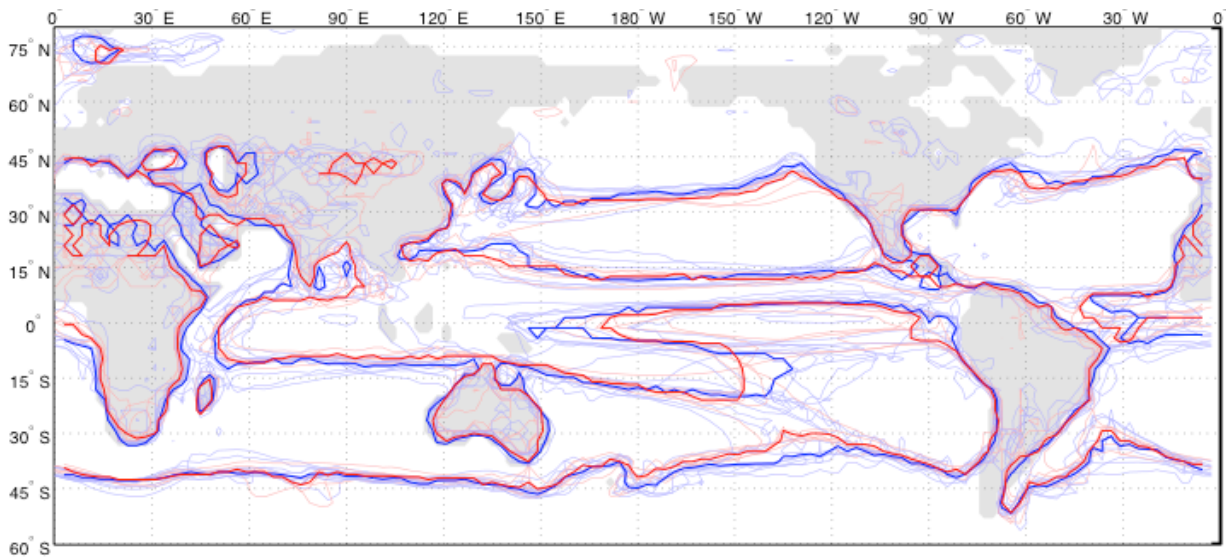
449  
450  
451



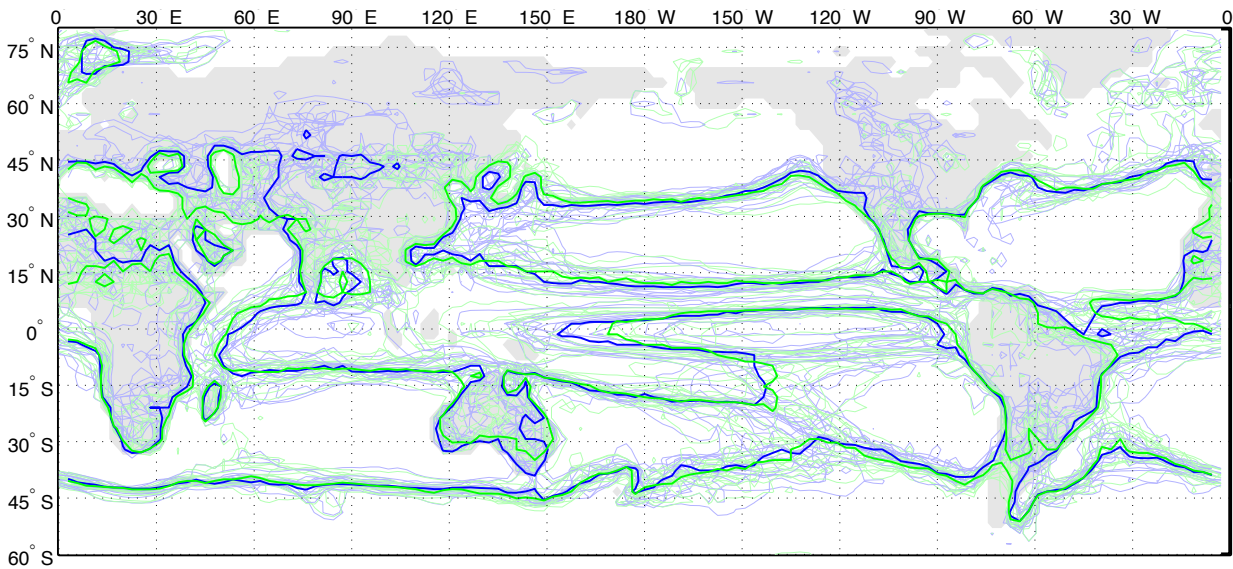
452  
453  
454  
455  
456  
457  
458

**Figure 3.** Simulated future changes in global atmospheric moisture transport from ocean to land for CMIP3 climate models. Shown are linear trends of annual mean moisture transport in blue bars and linear trends of annual mean residuals in the atmospheric moisture budgets in orange bars. The calculations were performed with the combined time series of the 20<sup>th</sup> and 21<sup>st</sup> (A2) century scenarios.

## Global water cycle assessment in CMIP3 climate models



459



460

461

**Figure 4.** Predicted long-term mean positions of dry zone edges of the 21<sup>st</sup> century (A2) scenario for

462

CMIP3 climate models. Top) 21<sup>st</sup> century multi-model means for two subsets of models. In red are the

463

contours of models with artificial leaking (globally negative atmospheric moisture imbalance) and in blue

464

with artificial flooding of the atmospheres (globally positive atmospheric moisture imbalance). Bottom) 21<sup>st</sup>

465

century multi-model means for two 20-year periods. In green are the contours of the dry-zone edges from

466

the means of the last two (2081 – 2100) and in blue for the first two decades (2001 – 2020). Shown are the

467

contour lines of balanced atmospheric moisture budget, which corresponds to  $E = P$ , where evaporation

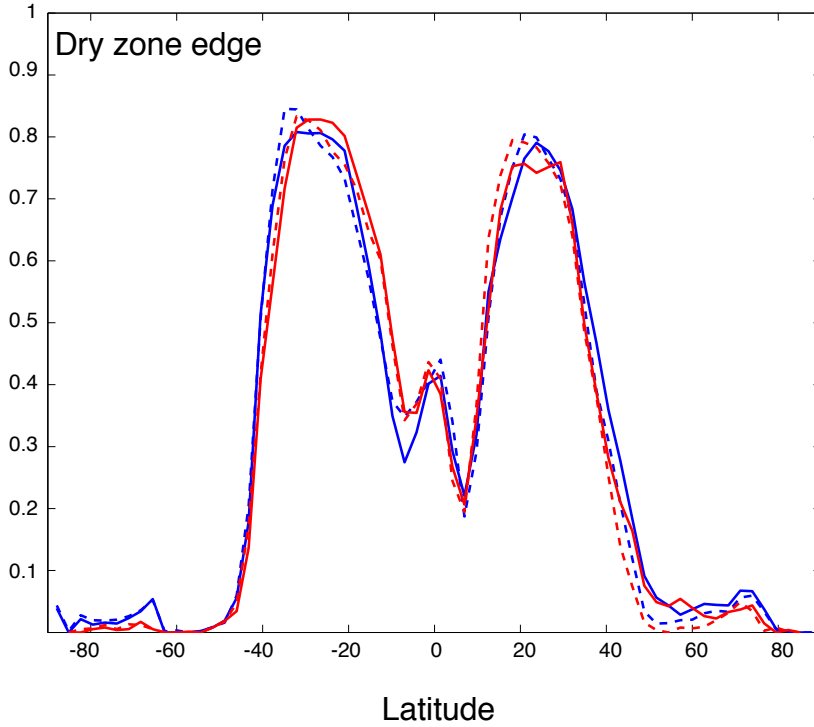
468

equals precipitation. The thick contour lines represent the multi-model composites of dry-zone edges of the

469

corresponding subsets.





470 **Figure 5.** The four curves represent the zonal mean positions of CMIP3 multi-model mean dry zone edges  
 471 of the first (full line) and last (dashed line) 20-year periods of the 21<sup>st</sup> century A2 scenario. The multi-model  
 472 means are separated into subsets of artificially leaking (globally negative atmospheric moisture imbalance)  
 473 models in red and flooding (globally positive atmospheric moisture imbalance) models in blue. The zonal  
 474 means are calculated for the atmospheric moisture budgets, with value ‘zero’ set for grid boxes where  $E <$   
 475  $P$ , and value ‘one’ set  $E \geq P$ .